Incomplete ionization of aluminum in silicon and its effect on accurate determination of doping profiles

Michael Rauer,[1,a)] Marc Rüdiger,[1] Christian Schmiga,[1] Hartmuth Strutzberg,[2] Mario Bähr,[2] Markus Glatthaar,[1] and Stefan W. Glunz[1]
[1]*Fraunhofer Institute for Solar Energy Systems (ISE), Heidenhofstrasse 2, 79110 Freiburg, Germany*
[2]*CiS Forschungsinstitut für Mikrosensorik und Photovoltaik, Konrad-Zuse-Straße 14, 99099 Erfurt, Germany*

(Received 1 October 2013; accepted 8 November 2013; published online 25 November 2013)

We present a detailed study on incomplete ionization (i.i.) of aluminum acceptors in highly aluminum-doped p^+ silicon formed by alloying from screen-printed Al pastes. We apply electrochemical capacitance-voltage (ECV) and secondary ion mass spectrometry (SIMS) measurements to detect the Al doping profiles and discuss key aspects necessary for a precise determination of the profiles. The excellent accordance of ECV- and SIMS-measured acceptor profile curves allows for the accurate investigation of Al acceptor ionization. We review the physics of i.i. and verify a simple quantitative model for incomplete Al acceptor ionization by comparing measured and calculated sheet-resistances of Al-doped p^+ Si surfaces. We thus show that the electrically active Al doping concentration is nearly two times lower than the total Al concentration, so that i.i. of Al acceptors has to be considered for the correct description of highly Al-doped p^+ Si regions. Therefore, our results allow for an improved quantitative analysis of n- and p-type silicon solar cells with Al-alloyed p^+ rear emitter or back surface field, respectively.
© *2013 AIP Publishing LLC*. [http://dx.doi.org/10.1063/1.4833242]

I. INTRODUCTION

For the optimization of n- or p-type silicon solar cells with aluminum-alloyed p^+ rear emitter[1–5] and back surface field,[6–8] respectively, the electrical properties of the Al-doped p^+ Si (Al-p^+) regions are highly important, as has been demonstrated by experiments[9–11] and simulations.[12,13] Typical acceptor concentrations of Al-p^+ regions formed in Si by alloying of screen-printed Al paste are in the range of $7 \cdot 10^{17}$ to $5 \cdot 10^{18}\,\mathrm{cm}^{-3}$ (Refs. 14 and 15), which is relevant for incomplete ionization (i.i.) of dopant atoms.[16–18] I.i. is thereby caused by the approaching of the Fermi level and the Al acceptor level, resulting in the restriction of holes to localized Al acceptor states, which prevents free hole movement. Although the theory of i.i. has been intensively studied[19–21] and is well-known today, it has been unclear if it also applies for Al acceptors formed by alloying. Huster *et al.* have published first investigations on i.i. in Al-p^+ regions, showing that i.i. has to be taken into account and pointing out that the high ionization energy of Al acceptors in Si ($E^0_{\mathrm{dop,Al}} = 69\,\mathrm{meV}$ (Ref. 22)) leads to a strong effect.[16] Furthermore, they presented a qualitative dependency of the ionization percentage from the doping concentration.[16] Focusing on the recombination properties of Al-p^+ regions, which strongly depend on the concentration of ionized Al acceptors, we have recently introduced a quantitative description of i.i. based on a physical model implemented in Sentaurus Device. By implementing i.i. of Al acceptors, we could calculate the recombination current densities of both non-passivated and surface-passivated Al-p^+ regions in excellent accordance to experimental data.[13]

In this study, we use an alternative and direct approach to evaluate the quantitative model for i.i. of Al acceptors. We compare the electrically active Al concentration with the total Al concentration by measuring and calculating Al-p^+ region resistivities as introduced by Huster *et al.* Furthermore, we review and discuss the underlying physics in detail. For investigating i.i. of Al-p^+ regions, a correct assessment of the Al acceptor profiles is crucial. We therefore focus on the accurate determination of Al acceptor profiles and compare different measurement techniques.

II. SAMPLE FABRICATION

In the course of this work, we have fabricated simple test samples using shiny-etched (100)-oriented p-type boron-doped float-zone silicon wafers. After wet-chemical cleaning, a commercially available non-fritted Al paste was screen-printed onto one entire wafer surface and dried to remove the solvents (Al paste amount exceeding $14\,\mathrm{mg/cm}^2$ after drying). Subsequently, the Al-p^+ region was alloyed in a fast firing furnace at a peak temperature of 900 °C. Different peak temperature times have been applied to realize a variation of the Al-p^+ region thickness.[10,23] Then, the paste residuals and the Al-Si eutectic layer were etched off in hydrochloric acid to lay open the Al-p^+ surface. To further remove pyramidal Al-containing structures from the Al-p^+ surface,[10,24] one part of the samples was additionally etched in potassium hydroxide (KOH) solution.

III. ECV AND SIMS MEASUREMENTS OF Al-p^+ DOPING PROFILES

To characterize the Al-doped p^+ Si regions, we have carried out doping profile measurements using an electrochemical capacitance-voltage (ECV) profiler (WEP CVP21) with a diluted ammonium biflouride (NH_4HF_2) electrolyte.

a)Electronic mail: michael.rauer@ise.fraunhofer.de

 © 2013 AIP Publishing LLC

[This article is copyrighted as indicated in the article. Reuse of AIP content is subject to the terms at: http://scitation.aip.org/termsconditions. Downloaded to] IP: 128.172.10.194 On: Tue, 24 Jun 2014 10:53:57

The ECV technique provides a very accurate profiling method, if the measurement unit is calibrated thoroughly.[16,25] In the following, we review important aspects that have to be taken into account for a correct profile curve determination: (i) The diameter of the sealing ring, (ii) the etch crater walls, (iii) the surface roughness, and (iv) the contact depth. In Figure 1, these aspects are schematically shown.

(i) **Sealing ring diameter**: ECV is extremely sensitive to the measuring area between electrolyte and sample surface, which is defined by a sealing ring. Thus, the diameter of the sealing ring has to be controlled externally as reported by Bock *et al.*[25] We have determined a diameter of 3.55 ± 0.06 mm using a surface profiler Dektak 6M and an optical microscope, resulting in a small correction of $1.7\%_{rel}$ on the doping profiles.

(ii) **Etch crater walls**: Huster *et al.* pointed out that the etch crater walls also contribute to the measuring area, in particular for measured depths of several micrometer.[16] We have observed that this effect is slightly amplified by underetching of the sealing ring during the measurement due to the isotropic etching of the NH_4HF_2 electrolyte, leading to sloped crater walls. However, due to the large diameter of the sealing ring applied in this study, the contribution of the etch crater walls to the measuring area is only marginal, leading to an area enlargement of approximately $2\%_{rel}$ for etching depths of 15 μm.
Please note that the doping concentration gradient along the crater may additionally influence the ECV measurement.[16] As the gradient of Al doping profiles formed by alloying is small,[10,15,16,24] we have calculated a negligible effect on the concentration of maximal $1\%_{rel}$.

(iii) **Surface roughness**: The most critical aspect for precise ECV measurements is the correction of the surface roughness.[16] For surfaces exhibiting a distinct roughness, the contact area is not defined by the sealing ring area A_{ring} but by the roughness-enlarged surface area A_{surf}, so that the measured acceptor concentration $N_{Al,meas}$ overestimates the actual Al concentration N_{Al} (Refs. 16 and 26)

$$N_{Al} = \left(\frac{A_{ring}}{A_{surf}}\right)^2 \times N_{Al,meas}. \quad (1)$$

For Al-p^+ regions formed by alloying, a certain roughness is inevitably induced during the Al alloying process. The degree of roughness thereby considerably depends on the printing and alloying conditions; e.g., the less Al paste is applied, the rougher the surface becomes.[10,15,16] The correction term depends on the square of the area ratio, so that underestimating the contact area can lead to a significant overrating of the Al acceptor concentration.
In this study, we have printed high Al paste amounts and adapted the firing conditions in order to achieve roughness-induced Al-p^+ surface enlargements below approximately $2\%_{rel}$, which has been determined by confocal microscopy.

(iv) **Crater depth**: During ECV measurements, the depth of the etch crater is automatically logged by temporally integrating the etching current and applying Faraday's law.[27] However, this can lead to systematic errors for the etch depth, in particular for deep profiles as presented by Bock *et al.*[25] Therefore, we have corrected each profile by remeasuring the etch crater depths and applying a correction of up to $15\%_{rel}$.

Figure 2 shows a typical ECV-measured Al doping profile of an alloyed Al-p^+ Si region after carrying out the above mentioned corrections. In contrast to diffusion of boron or phosphorus in silicon, e.g., the Al-doped region is formed during alloying by the incorporation of Al atoms into the lattice of Si recrystallizing epitaxially at the Si bulk surface.[28] Al doping profiles are therefore defined by the solubility of Al in crystalline Si, which is particularly dependent on the temperature. As a consequence, the doping concentrations

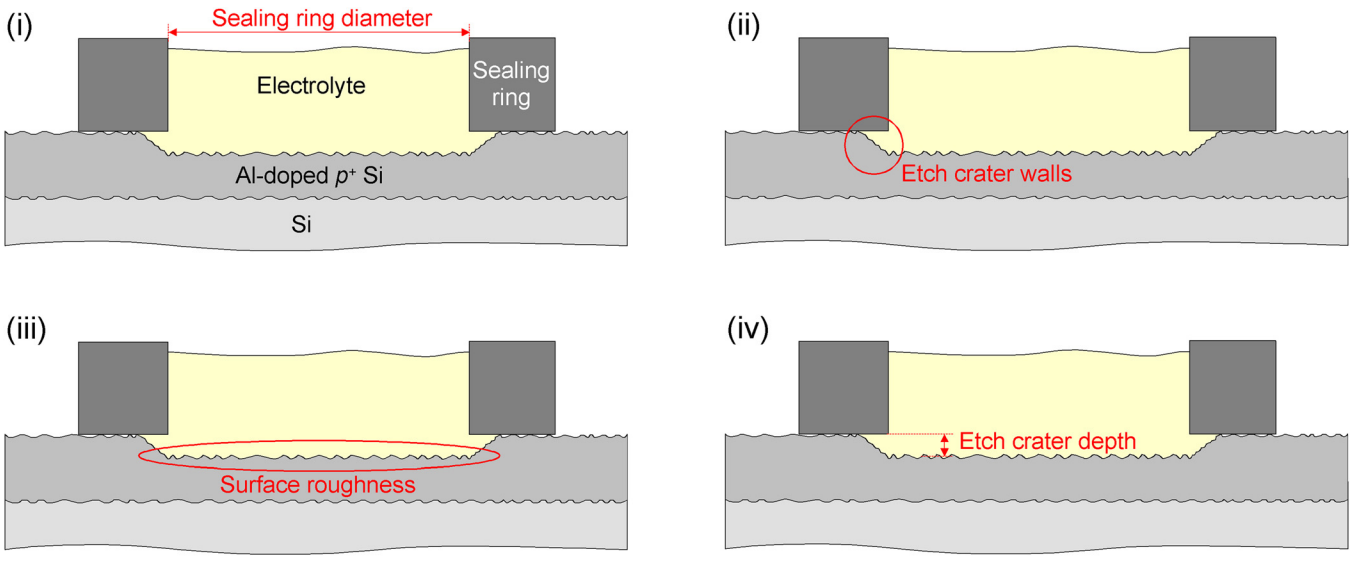

FIG. 1. Schematic cross-sections of the electrolyte/Al-doped p^+ Si contact during ECV measuring, demonstrating the aspects that have to be taken into account for an accurate determination of the doping profile.

[This article is copyrighted as indicated in the article. Reuse of AIP content is subject to the terms at: http://scitation.aip.org/termsconditions. Downloaded to] IP: 128.172.10.194 On: Tue, 24 Jun 2014 10:53:57

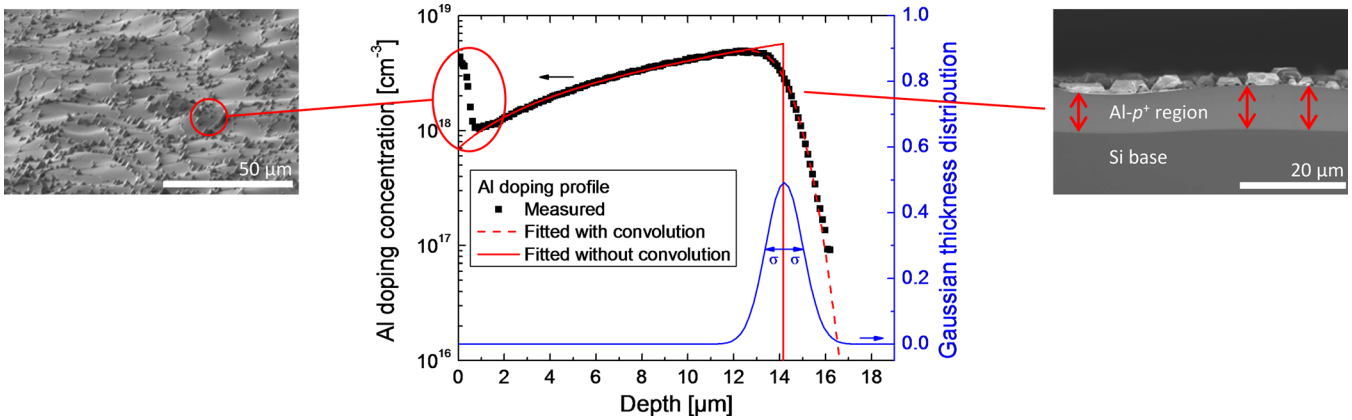

FIG. 2. ECV measurement of a typical Al doping profile formed by alloying. Artifacts: (i) surface-near concentration peak: pyramidal structures, (ii) blurred decrease at Al-p^+/Si base transition: thickness inhomogeneities. The measured profiles (squares) can be fitted (dashed red line) by assuming a convolution of the actual doping profile (solid red line) with a Gaussian thickness distribution for the Al-doped p^+ Si region (solid blue line). The tilted (left) and cross-sectional (right) scanning electron microscopy images of the Al-p^+ region illustrate the occurrence of the artifact.

are in the range of $7 \cdot 10^{17}$ to $5 \cdot 10^{18}\,\mathrm{cm}^{-3}$ and the doping profiles exhibit an exponential increase from the Al-p^+ region surfaces to the Al-p^+ region/Si bulk interface.

In addition, two features characteristic for ECV measurements of Al doping profiles formed by alloying appear, see Figure 2:

(i) The concentration peak at the surface of the Al doping profile can be attributed to pyramidal structures,[10,24] which are caused by the characteristic lamellar structure of the Al-Si eutectic.[15] These structures lead to a significant enlargement of the ECV measuring area,[24] so that the concentration peak at the surface is considered to be a measurement artifact. After removing the pyramidal structures by a short dip in KOH solution, this peak vanishes.[10,24] Please note that for the determination of the Al-p^+ region roughness correction, the pyramidal structures have not been taken into account.

(ii) The rounded shape of the Al doping profile curve at the transition to the Si base is caused by a variation of the Al-p^+ thickness within the ECV measuring area.[16]

Therefore, the Al doping profiles can be fitted by neglecting the high values near the surface and assuming a convolution of an abrupt doping profile and a Gaussian thickness distribution,[13,16] see Figure 2. The abrupt, non-convoluted profile then represents the actual, area-averaged Al doping profile, which is used for further investigations.

Finally, it is important to consider what is actually detected by ECV measurements.[16] The ECV technique is based on modulating an external voltage on the electrolyte/Si Schottky contact, which creates a space charge (SC) region within the silicon. By varying the external voltage, the depth and thus the capacitance of the SC region varies, depending on the doping concentration in the vicinity of the SC edge,[26] so that the latter can be determined. The strong band bending within the SC region thereby leads to the ionization of originally non-ionized, electrically inactive dopant atoms that are substitutionally incorporated in the Si crystal. Thus, all substitutional dopant atoms contribute to the ECV doping profile.[29] Consequently, for Al-p^+ regions formed by alloying, the ECV technique does not detect the electrically active, but the total Al concentration. Please note that it is important to distinguish between electrically inactive, substitutional, and non-substitutional dopant atoms. Non-substitutional dopant atoms, as agglomerated or precipitated phosphorus atoms exceeding the activation or solubility limit,[30] are not ionized and thus are not measured by ECV.[31]

In order to validate our ECV calibration, we have additionally carried out quantitative secondary ion mass spectrometry (SIMS) measurements of Al-alloyed p^+ regions. The SIMS technique, which exhibits a measurement spot with a diameter of only $8\,\mu\mathrm{m}$, is based on sputtering the Al-p^+ surface by O_2^+ ion bombardment and analyzing the sputtered secondary ions by means of mass spectrometry, so that the total Al concentration is detected.

For the SIMS measurement, the Al profile samples have to be prepared very carefully: The SIMS technique is very sensitive to surface roughness and the change in angle of ion incidence that is accompanied by rough surfaces.[32] In contrast to ECV, where the profiles can easily be corrected for the surface roughness after the measurements, during SIMS measurements, rough surfaces severely affect the yield of secondary ions and limit the depth resolution.[32] Moreover, an additional roughening of the surface can occur during sputtering, which is promoted by an initially rough Al-p^+ surface and leads to the formation of rough, periodically modulated structures named *ripples*.[32,33] It has been reported in literature that the amplitude of these ripples increases with increasing etch depth,[33] thus causing large measurement errors for high Al-p^+ region thicknesses. Consequently, the samples for proper SIMS measurements should exhibit a thin and simultaneously very smooth Al-p^+ region. We have observed that reliable measurements can be performed for Al-p^+ region thicknesses up to approximately $5\,\mu\mathrm{m}$.

It has recently been shown that the formation of smooth Al-p^+ regions is directly correlated with applying high Al paste amounts.[15,16,34,35] We therefore have fabricated test samples using the process sequence described in Sec. II and applying an Al paste amount of $21.7\,\mathrm{mg/cm}^2$. As smooth and continuous Al-p^+ regions are only formed for higher thicknesses though,[15,16] thin Al-p^+ regions cannot be realized by applying high Al paste amounts and solely adjusting the

[This article is copyrighted as indicated in the article. Reuse of AIP content is subject to the terms at: http://scitation.aip.org/termsconditions. Downloaded to] IP: 128.172.10.194 On: Tue, 24 Jun 2014 10:53:57

alloying conditions. Instead, we prepared an Al-p^+ region with a rather high thickness of 12.0 μm and homogeneously thinned down the Al-doped region by wet-chemical etching. We could thus realize a smooth Al-p^+ region with a thickness of 5.4 μm, exhibiting a thickness standard deviation of only 0.6 μm.

Figure 3 shows an ECV measurement, corrected as described above, and three SIMS measurements of the Al acceptor profile on one sample, taken at different positions only few millimeters apart. After thoroughly preparing the sample and calibrating the ECV setup, we achieve excellent accordance of both measurement techniques.

Two interesting aspects occur here: The SIMS technique exhibits a much smaller measurement spot with a diameter of only 8 μm, so that there virtually is no variation of the Al-p^+ thickness within the measurement area, resulting in a very narrow thickness distribution. Thus, the SIMS-measured Al dopant profiles show a much more abrupt Al-p^+/Si base transition. Due to the small measurement area, however, SIMS measurements are significantly more sensitive to lateral Al-p^+ region thickness variations, as there is practically no area averaging effect. This can also be seen at the variation of the profile depths detected by SIMS at different positions on the sample.

In conclusion, we have shown that, after thorough calibration, our ECV setup allows for accurate measurements of Al doping profiles formed by alloying from screen-printed Al pastes. Moreover, the good accordance of ECV- and SIMS-measured doping concentrations shows (i) that the Al atoms are incorporated substitutionally into the Si during alloying and (ii) that ECV detects the total Al dopant concentration by ionizing electrically inactive dopant atoms. For a solar cell in operation conditions, the electrical properties though are determined by the ionized, electrically active dopant atoms, so that the following sections will deal with reviewing the physics of incomplete Al acceptor ionization and experimentally evaluating a simple quantitative model for i.i.

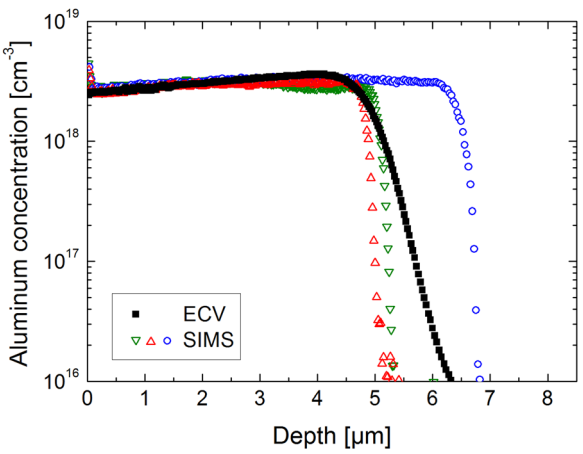

FIG. 3. Al acceptor concentration profiles of an Al-doped p^+ region measured via ECV (closed symbols) and SIMS (open symbols). The SIMS measurements were carried out at three different positions on the sample. As the SIMS technique exhibits a significantly smaller measurement spot (diameter 8 μm) than the ECV technique (diameter 3.55 ± 0.06 mm), (i) the decrease of the Al profile towards the Si bulk is more abrupt due to less Al-p^+ thickness variations within the measurement area and (ii) SIMS is more sensitive to lateral thickness variations, resulting in different Al-p^+ thicknesses for the measurements at different positions.

IV. INCOMPLETE IONIZATION OF AL ACCEPTOR ATOMS

We have recently shown that i.i. of Al acceptors has to be taken into account to accurately model the recombination properties of Al-p^+ regions formed by alloying of Al pastes.[13]

When increasing the Al acceptor concentration N_{Al} within the Si crystal, the Coulomb interaction between the Al acceptors increases, leading to (i) the broadening of the Al acceptor energy level into an acceptor band and (ii) the approaching of the acceptor band to the valence band edge (with energy E_{V}).[17,21] As exhibiting a minor effect on i.i., the broadening into an acceptor band can be neglected and the acceptor energy levels can be treated as a discrete acceptor level with an energy $E_{\mathrm{V}} + E_{\mathrm{dop,Al}}$.[17,18] The approaching of the acceptor level to the valence band edge is then equivalent to a decrease of the acceptor energy $E_{\mathrm{dop,Al}}$ with increasing Al concentration N_{Al}. This decrease is caused by a decrease of the potential energy of attraction between the acceptor atoms and holes due to shielding by other mobile valence band holes.[19,20,36] Thus, it is inversely proportional to the average distance between the acceptors, which can be expressed by $N_{Al}^{-1/3}$,[36] so that the doping energy follows an equation of the type:[37,38]

$$E_{\mathrm{dop,Al}}(N_{\mathrm{Al}}) = E^0_{\mathrm{dop,Al}} - \alpha \cdot N_{\mathrm{Al}}^{1/3}. \tag{2}$$

The proportionality factor α was determined to be $3.1 \cdot 10^{-5}$ meVcm.[37,38] For low Al concentrations, an Al dopant energy $E^0_{\mathrm{dop,Al}}$ value of 69.0 meV has been reported.[22]

When increasing the Al acceptor concentration, the Fermi level exhibiting the energy $E_{\mathrm{V}} + E_{\mathrm{F}}$ also approaches the valence band edge,[39] i.e., E_{F} decreases. As the decrease of E_{F} occurs faster than the decrease of $E_{\mathrm{dop,Al}}$, an increasing part of holes is restricted to localized Al acceptor states. Thus, the fraction f_{Al} of ionized Al acceptor atoms decreases. By assuming Boltzmann statistics, f_{Al} can be assessed by[39]

$$f_{\mathrm{Al}}(N_{\mathrm{Al}}) = \frac{1}{1 + g_{\mathrm{A}} \cdot \exp\left(\dfrac{E_{\mathrm{dop,Al}}(N_{\mathrm{Al}}) - E_{\mathrm{F}}(N_{\mathrm{Al}})}{k_{\mathrm{B}}T}\right)} \quad \text{for} \quad N_{\mathrm{Al}} < N_{\mathrm{Al,crit}} \tag{3}$$

with a degeneracy factor $g_{\mathrm{A}} = 4$.[39] To iteratively solve this equation, we have used Sentaurus TCAD.[13] Figure 4(a) shows f_{Al} in dependence of the Al concentration N_{Al}, demonstrating that i.i. of Al acceptors can amount up to 55%.

For Al concentrations exceeding $1.1 \cdot 10^{19}\,\mathrm{cm}^{-3}$, the acceptor energy $E_{\mathrm{dop,Al}}$ vanishes, indicating the Mott insulator-metal transition.[17,40] Here, the acceptor level merges with the valence band, enabling free hole movement and leading to complete Al ionization for doping concentrations above this critical value. As no further values for the critical Al concentration have been published, we use $N_{\mathrm{Al,crit}} = 1.1 \cdot 10^{19}\,\mathrm{cm}^{-3}$, which is consistent with literature

[This article is copyrighted as indicated in the article. Reuse of AIP content is subject to the terms at: http://scitation.aip.org/termsconditions. Downloaded to] IP: 128.172.10.194 On: Tue, 24 Jun 2014 10:53:57

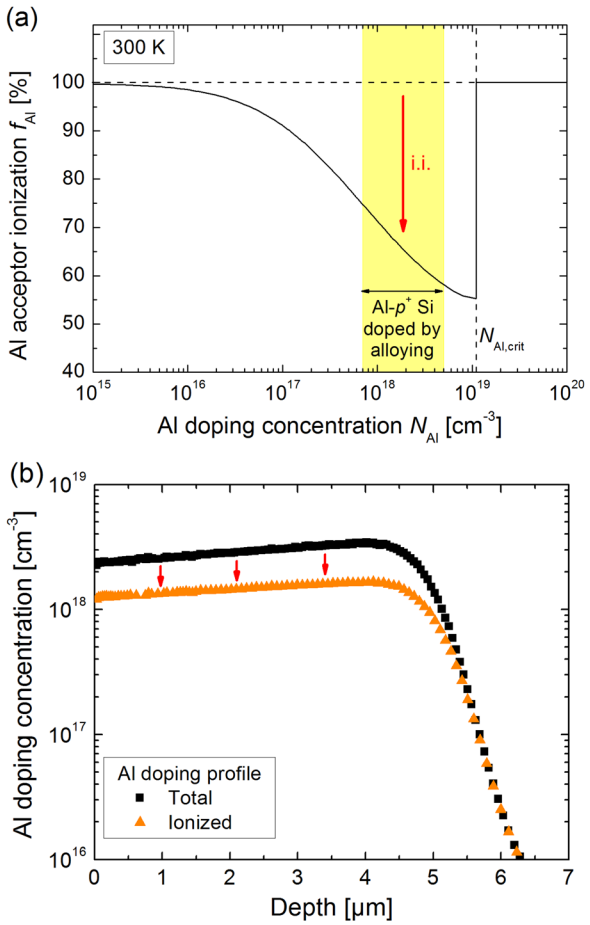

FIG. 4. (a) Calculated ionization of Al acceptor atoms f_{Al} as a function of the Al doping concentration N_{Al} in silicon.[13] With increasing N_{Al}, the Fermi level approaches the Al acceptor level, leading to the enhanced restriction of holes to localized Al acceptor states. Thus, the fraction of ionized Al acceptors decreases. Above $N_{Al,crit}$, the Al doping energy vanishes, resulting once again in complete ionization. For Al-p^+ Si doped by alloying only 75% to 55% of the Al acceptor atoms are ionized in the relevant doping range. (b) Total (circles) and ionized (triangles) Al acceptor concentration of the Al profile displayed in Figure 3.

data for the Mott transitions of other dopant species in silicon.[18] Using a constant value for g_A, which is particularly independent of N_{Al}, causes a monotonous increase of i.i. with N_{Al} and an unphysically hard transition to complete ionization above $N_{Al,crit}$.[18] However, since Al doping concentrations within this study are well below $N_{Al,crit}$, we expect only minor deviations for Al-p^+ regions formed by alloying of screen-printed Al paste.

In conclusion, in order to assess the ionized, electrically active Al acceptor concentration, relevant for solar cell operation, N_{Al} has to be multiplied by f_{Al}, leading to a significant shift of the profile. Figure 4(b) shows the total and the ionized Al acceptor concentration of the Al-p^+ profile already displayed in Figure 3.

V. SHEET RESISTANCE MEASUREMENTS

For validating the model for incomplete Al acceptor ionization, a method to compare the ionized, i.e., the electrically active with the complete Al doping concentration is required. As introduced by Huster *et al.*,[16] we use the four-point probe (4PP) technique to measure the electrical sheet resistance $\rho_{sh,4PP}$ of the Al-doped Si region and the ECV method to determine the Al concentration N_{Al}. We calculate $\rho_{sh,ECV}$ using

$$\rho_{sh,ECV} = \frac{d_{Al-p+}}{e \cdot \int_0^{d_{Al-p+}} \mu_p(N_{Al}(z)) \cdot N_{Al}(z)\ dz}. \quad (4)$$

Here, e stands for the elementary charge, μ_p for the hole mobility[41] and d_{Al-p+} for the thickness of the abrupt, non-convoluted Al-p^+ doping profile, see Sec. III. As the ECV technique measures the total Al concentration, $\rho_{sh,ECV}$ is a theoretical lower boundary for the Al-p^+ sheet resistance in case of complete ionization. Figure 5 displays the measured 4PP and calculated ECV sheet resistances for thirteen samples fabricated under various alloying conditions, comprising a broad range of sheet resistances. We thereby distinguish between samples with and without surface structures. A significant gap between the measured and calculated values appears, which indicates that the ECV-measured Al doping concentration clearly overestimates the electrically active concentration.

In order to account for incomplete ionization according to the model of Sec. IV, N_{Al} has to be replaced by $N_{Al} \cdot f_{Al}$ in Eq. (4). Thus, the sheet resistances calculated from the ECV measurements are in acceptable agreement with the values measured by 4PP, see Figure 5. The slight undervaluation for samples exhibiting surface structures may be attributed to the

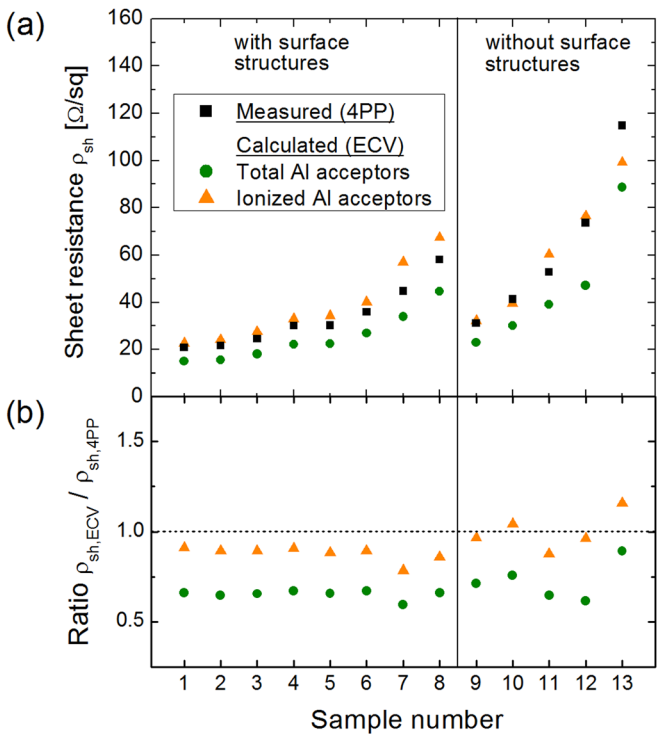

FIG. 5. (a) Sheet resistances of Al-doped p^+ Si regions with and without surface structures, respectively. The sheet resistances have been measured by the 4PP technique (circles) and calculated from ECV doping profiles, thereby assuming complete (squares) and incomplete Al ionization (triangles). (b) Ratio of calculated and measured sheet resistances. Good accordance of measured and calculated data is obtained by considering i.i.

[This article is copyrighted as indicated in the article. Reuse of AIP content is subject to the terms at: http://scitation.aip.org/termsconditions. Downloaded to] IP: 128.172.10.194 On: Tue, 24 Jun 2014 10:53:57

structures themselves, which complicate the determination of the actual Al doping profile and possibly modify the ECV measurement beyond the surface doping peak as well. In summary, the calculations show that incomplete ionization can amount up to approximately 55% and, therefore, has to be taken into account for the correct assessment of highly Al-doped p^+ regions in silicon.

VI. SUMMARY

We have shown that incomplete ionization significantly affects the conductivity of highly Al-doped silicon and has to be taken into account for the accurate description of Al-alloyed p^+ Si regions.

By carefully calibrating the ECV measurements, the Al doping concentrations of various Al-doped p^+ Si regions have been determined with high accuracy. We demonstrate excellent accordance of SIMS- and ECV-measured Al profile curves and, thus, prove that the Al atoms are incorporated substitutionally during alloying. In conclusion, we demonstrate that the ECV method measures the total Al concentration.

For assessing incomplete Al acceptor ionization, we have evaluated a quantitative model, which has recently been introduced, and have compared sheet-resistances calculated from the total Al doping profiles with values measured by the four-point probe technique. Significant differences indicate that the electrically active Al doping concentration is nearly 50% lower than the total Al concentration. By implementing a correction for incomplete Al ionization given by the quantitative model, a good accordance between measured and calculated sheet resistances was achieved.

ACKNOWLEDGMENTS

The authors would like to thank all colleagues of Fraunhofer ISE cleanroom and PV-TEC team and all other members of SEC department for their contributions to this work. Michael Rauer wants to thank the Reiner Lemoine Stiftung for funding.

[1]D. L. Meier, H. P. Davis, R. A. Garcia, J. Salami, A. Rohatgi, A. Ebong, and P. Doshi, Sol. Energy Mater. Sol. Cells **65**, 621–627 (2001).
[2]C. Schmiga, H. Nagel, and J. Schmidt, Prog. Photovoltaics **14**(6), 533–539 (2006).
[3]F. Book, T. Wiedenmann, G. Schubert, H. Plagwitz, and G. Hahn, Energy Proc. **8**(8), 487–492 (2011).
[4]C. Schmiga, M. Rauer, M. Rüdiger, M. Glatthaar, and S. W. Glunz, paper presented at the 27th European Photovoltaic Solar Energy Conference and Exhibition, Frankfurt, Germany (2012), pp. 915–918.
[5]M. Rauer, A. Mondon, C. Schmiga, J. Bartsch, M. Glatthaar, and S. W. Glunz, Energy Proc. **38**, 449–458 (2013).
[6]S. W. Glunz, R. Preu, and D. Biro, in *Comprehensive Renewable Energy*, edited by A. Sayigh (Elsevier, Oxford, 2012), Vol. 1, pp. 353–387.
[7]B. Tjahjono, H. Haverkamp, V. Wu, H. T. Anditsch, W.-H. Jung, J. Cheng, J. Ting, M. J. Yang, D. Habermann, T. Sziptalak, C. Buchner, C. Schmid, B. Beilby, and K.-C. Hsu, paper presented at the 26th European Photovoltaic Solar Energy Conference and Exhibition, Hamburg, Germany (2011), pp. 901–905.
[8]B. Hallam, S. Wenham, A. Sugianto, L. Mai, C. Chong, M. Edwards, D. Jordan, and P. Fath, IEEE J. Photovolt. **1**(1), 43–48 (2011).
[9]C. Schmiga, M. Rauer, M. Rüdiger, K. Meyer, J. Lossen, H.-J. Krokoszinski, M. Hermle, and S. W. Glunz, paper presented at the 25th European Photovoltaic Solar Energy Conference and Exhibition, Valencia, Spain (2010), pp. 1163–1168.
[10]M. Rauer, C. Schmiga, M. Hermle, and S. W. Glunz, paper presented at the 24th European Photovoltaic Solar Energy Conference, Hamburg, Germany (2009), pp. 1059–1062.
[11]J. Müller, K. Bothe, S. Gatz, H. Plagwitz, G. Schubert, and R. Brendel, IEEE Trans. Electron Devices **58**(10), 3239–3245 (2011).
[12]M. P. Godlewski, C. R. Baraona, and H. W. Brandhorst, Jr., paper presented at the 10th IEEE Photovoltaic Specialists Conference, Palo Alto, California, USA (1973), pp. 40–49.
[13]M. Rüdiger, M. Rauer, C. Schmiga, and M. Hermle, J. Appl. Phys. **110**, 024508 (2011).
[14]T. Yoshikawa and K. Morita, J. Electrochem. Soc. **150**(8), G465–G468 (2003).
[15]J. Krause, R. Woehl, M. Rauer, C. Schmiga, J. Wilde, and D. Biro, Sol. Energy Mater. Sol. Cells **95**(8), 2151–2160 (2011).
[16]F. Huster and G. Schubert, paper presented at the 20th European Photovoltaic Solar Energy Conference, Barcelona, Spain (2005), pp. 1462–1465.
[17]P. P. Altermatt, A. Schenk, and G. Heiser, J. Appl. Phys. **100**(11), 113714 (2006).
[18]P. P. Altermatt, A. Schenk, B. Schmithusen, and G. Heiser, J. Appl. Phys. **100**(11), 113715 (2006).
[19]G. W. Castellan and F. Seitz, in *Semi-Conducting Materials* (Butterworths Scientific Publications, London, 1951), pp. 8–25.
[20]P. P. Debye and E. M. Conwell, Phys. Rev. B. **93**(4), 693 (1954).
[21]R. Riklund and K. A. Chao, Phys. Rev. B. **26**(4), 2168 (1982).
[22]D. W. Fischer and J. J. Rome, Phys. Rev. B **27**(8), 4826–4832 (1983).
[23]M. Rauer, C. Schmiga, M. Hermle, and S. W. Glunz, Phys. Status Solidi A **207**, 1249–1251 (2009).
[24]R. Bock, J. Schmidt, R. Brendel, H. Schuhmann, and M. Seibt, J. Appl. Phys. **104**(4), 043701 (2008).
[25]R. Bock, P. P. Altermatt, and J. Schmidt, paper presented at the 23rd European Photovoltaic Solar Energy Conference, Valencia, Spain (2008), pp. 1510–1513.
[26]P. Blood, Semicond. Sci. Technol. **1**, 7–27 (1986).
[27]E. Peiner, A. Schlachetzki, and D. Krüger, J. Electrochem. Soc. **142**(2), 576 (1995).
[28]P. Lölgen, C. Leguijt, J. A. Eikelboom, R. A. Steeman, W. C. Sinke, L. A. Verhoef, P. F. A. Alkemade, and E. Algra, paper presented at the 23rd IEEE Photovoltaic Specialists Conference, Louisville, Kentucky, USA (1993), pp. 236–242.
[29]T. J. Woodley and C. T. Sah, Solid-State Electron. **20**, 385 (1977).
[30]S. Solmi, A. Parisini, R. Angelucci, A. Armigliato, D. Nobili, and L. Moro, Phys. Rev. B **53**(12), 7836–7841 (1996).
[31]H. Wagner, A. Dastgheib-Shirazi, R. Chen, S. T. Dunham, M. Kessler, and P. P. Altermatt, paper presented at the 37th IEEE Photovoltaic Specialists Conference, Seattle, Washington (2011), pp. 2957–2962.
[32]S. Hofmann, Appl. Surf. Sci. **70–71**, 9–19 (1993).
[33]M. A. Makeev, R. Cuerno, and A.-L. Barabasi, Nucl. Instrum. Methods Phys. Res. B **197**, 185–227 (2002).
[34]M. Rauer, C. Schmiga, K. Meyer, J. Lossen, H.-J. Krokoszinski, M. Hermle, and S. W. Glunz, paper presented at the 25th European Photovoltaic Solar Energy Conference and Exhibition, Valencia, Spain (2010), pp. 1460–1464.
[35]J. Krause, R. Woehl, and D. Biro, paper presented at the 25th European Photovoltaic Solar Energy Conference and Exhibition, Valencia, Spain (2010), pp. 1899–1904.
[36]G. L. Pearson and J. Bardeen, Phys. Rev. B **75**(5), 865 (1949).
[37]A. Schenk, *Advanced Physical Models for Silicon Device Simulation* (Springer-Verlag, Wien, 1998).
[38]Sentaurus TCAD, Synopsys, Zürich, Switzerland, 2010.
[39]S. M. Sze, *Physics of Semiconductor Devices*, 2nd ed. (John Wiley & Sons, Inc., New York, 1981).
[40]P. Y. Yu and M. Cardona, *Fundamentals of Semiconductors*, 2nd ed. (Springer, Berlin, 2003).
[41]G. Masetti, M. Severi, and S. Solmi, IEEE Trans. Electron Devices **30**(7), 764–769 (1983).

[This article is copyrighted as indicated in the article. Reuse of AIP content is subject to the terms at: http://scitation.aip.org/termsconditions. Downloaded to] IP: 128.172.10.194 On: Tue, 24 Jun 2014 10:53:57